Review of Scientific Instruments ARTICLE scitation.org/journal/rsi

Probe measurements of electric field and electron density fluctuations at megahertz frequencies using in-shaft miniature circuits

Cite as: Rev. Sci. Instrum. 92, 033534 (2021); doi: 10.1063/5.0035135
Submitted: 26 October 2020 • Accepted: 28 February 2021 •
Published Online: 16 March 2021

Yibo Hu,[1,a] Jongsoo Yoo,[2] Hantao Ji,[2] Aaron Goodman,[2] and Xuemei Wu[1]

AFFILIATIONS

[1] School of Physical Science and Technology, Soochow University, Suzhou 215006, China
[2] Princeton Plasma Physics Laboratory, Princeton, New Jersey 08543, USA

[a] **Author to whom correspondence should be addressed:** huyibo3647@126.com

ABSTRACT

A four-tip electrostatic probe is constructed to measure high-frequency (0.1–10 MHz) fluctuations in both the electric field (one component) and electron density in a laboratory plasma. This probe also provides data for the local electron temperature and density. Circuits for high-frequency measurements are fabricated on two miniature boards, which are embedded in the probe shaft, near the tips to minimize the pickup of common-mode signals. The amplitude and phase response of two circuits to sinusoidal test signals are measured and compared with results from modeling. For both circuits, the phase shift between input and output signals is relatively small ($< 30^\circ$). The performance of the probe is verified in a high-density ($\sim 10^{13}$ cm^{-3}) and low-temperature ($\lesssim 10$ eV) plasma. The probe successfully measures high-frequency (~ 2 MHz) fluctuations in the electric field and density, which are associated with lower hybrid drift waves. This probe can provide information on the wave-associated anomalous drag, which can be compared with the classical resistivity.

I. INTRODUCTION

An electrostatic (Langmuir) probe is a useful tool usually used for measuring the electron temperature, density, and plasma potential. Common electrostatic probes are single, double, and triple probes.[1] Single and double probes can obtain the I–V curve by voltage sweeping. The triple probe,[2] on the other hand, does not require the voltage sweeping so that it can measure both the electron density and temperature with a much better time resolution. Thus, it is widely used in laboratory experiments where the plasma quantities change quickly.[1–4]

High-frequency fluctuations associated with various waves and instabilities in the plasma may impact on heating, transport, and relaxation processes in the plasma. For example, high-frequency fluctuations in the electric and magnetic fields are used to understand the impacts of lower hybrid drift waves (LHDWs) on magnetic reconnection.[5,6]

Simultaneous measurements of two different physical quantities are required to estimate wave-associated anomalous terms.[7,8] For example, measurements of high-frequency fluctuations in both the electric field and electron density are required to estimate anomalous momentum exchange between electrons and ions.[7] To quantify these anomalous terms, it is necessary to precisely measure both the amplitude and phase of fluctuations.

Here, we present a new four-tip electrostatic probe that can measure high-frequency fluctuations of the electric field (one component) and density as well as the average electron density and temperature. The primary purpose of this probe is not to identify the wave mode but to quantify effects of waves that have already been known. The tip configuration is based on the triple Langmuir probe. For minimizing noise pickup and impedance matching in the signal transmission line, two miniature circuit boards with buffer amplifiers are inserted into the probe shaft and located near the probe tips.[5,6,9] The detailed design of the probe and circuit with the target frequency range of 0.1–10 MHz is provided in Sec. II. Moreover, the probe performance is tested with sinusoidal (10 kHz–10 MHz) signals and compared with LT-Spice modeling. Finally, initial data from the probe near the reconnection region of a laboratory plasma are presented in Sec. III.

II. PROBE DESIGN AND CONSTRUCTION

A. Experimental considerations

This probe is designed to meet requirements for reconnection experiments in the Magnetic Reconnection Experiment (MRX),[10,11] a laboratory reconnection device located at the Princeton Plasma Physics Laboratory (PPPL). In MRX, a prototypical reconnection current sheet is generated near the center of the machine by using internal and external coils.[4,12,13] A list of parameters of typical helium plasma in MRX is provided in Table I. The electron gyroradius (ρ_e) is comparable to the probe dimension (~ 1 mm), while the ion gyroradius (ρ_i) is much larger.

The primary purpose of this probe is to measure the high-frequency fluctuations (up to 10 MHz) in the reconnection electric field component (E_{rec}) and electron density (n_e) in the reconnection current sheet of MRX. These high-frequency fluctuations are associated with lower hybrid drift waves.[5,6,14] Simultaneous measurements of δE_{rec} and δn_e are required to address wave-associated anomalous drag D, which is[7]

$$D = -\frac{\langle \delta n_e \delta E_{rec} \rangle}{\langle n_e \rangle}. \tag{1}$$

Here, $\langle \cdots \rangle$ denotes the average value of a physical parameter. To measure the anomalous drag, precise measurements of both the amplitude and phase of the fluctuating quantities are required.

The high-frequency fluctuation in E_{rec} is measured by two nearby floating tungsten tips,[5] which are separated by d = 3 mm. We measure the difference between two floating potentials (ΔV_f), from which the fluctuation in the electric field can be estimated as

$$E_{rec} \approx -\frac{\Delta V_f}{d}. \tag{2}$$

Ideally, we need to measure the plasma potential (V_p) at two tips ($E_{rec} = -\Delta V_p/d$), which requires emissive-type probes.[15] Emissive tips, however, require more complicated hardware and perturb the local plasma much more than floating tips. The relation between the plasma potential (V_p) and the floating potential is given as[3]

$$V_p - V_f = (3.3 + 0.5 \ln \mu) k T_e / e, \tag{3}$$

where k is the Boltzmann constant, T_e is the electron temperature in electron volts, and $\mu = m_i/m_p$ is the ratio of the ion mass to the proton mass. The use of V_f requires an assumption that the electron temperature does not vary over the probe separation; temperature fluctuations are ignored. With negligible ΔT_e, ΔV_f can represent ΔV_p. This assumption is justifiable in the current sheet of MRX, where the field component perpendicular to the direction along the probe separation becomes negligible such that the strong electron heat flux along the magnetic field direction minimizes the temperature difference.

TABLE I. Typical parameters for MRX discharges.

Parameters	Values
Density, n_{e0} (cm^{-3})	$1–10 \times 10^{13}$
Electron temperature, T_e (eV)	5–15
Ion temperature, T_i (eV)	7–15
Magnetic field, B_0 (G)	100–500
Lower hybrid frequency, f_{LH} (MHz)	3.3–16
Electron gyroradius, ρ_e (mm)	0.1–0.9
Ion gyroradius, ρ_i (mm)	10–79

For the density fluctuation measurement, two additional tips under the configuration of a double Langmuir probe are used. The bias voltage between two tips is 30–35 V, which is about three times larger than the typical electron temperature (~8–10 eV) in the current sheet. Then, the negative (V_-) tip draws the ion saturation current (I^+_{sat}). With unmagnetized ions, it is given by[16]

$$I^+_{sat} = 0.6 e n_e A C_s, \tag{4}$$

where n_e is the electron density, A = 2.8 mm^2 is the surface area of each probe tip, and C_s is the sound velocity. These four tips complete a triple Langmuir probe[2] so that the electron temperature can be obtained by $T_e = (V_+ - V_f)/\ln 2$,[1,2] where V_+ is the potential of the positive tip. This formula is valid when the bias voltage is much larger than the value of T_e (typically $V_B > 2T_e$). The sound velocity C_s is given by $\sqrt{T_e/m_i}$. We ignore the dependence of C_s on the ion temperature T_i since the ion saturation current does not strongly depend on T_i as long as $T_i < T_e$,[17] which is satisfied in MRX. With the known probe area A and measured sound velocity C_s, the electron density can be determined from I^+_{sat}.

B. Circuit design

Figure 1 shows the diagram of the probe tip configuration and the circuit. The circuit part in black is for δE_{rec} measurements. Two floating tips V_{f1} and V_{f2} are connected directly to a 1 : 1 pulse transformer (CX2041NLT, Pulse Electronics) that provides isolation from the plasma. The load resistor has a relatively high value ($R1 = R8 = 500\Omega$) to minimize both the current and the signal loss due to the sheath impedance of about 10 Ω. The rest part of the circuit is associated with a bipolar buffer amplifier ($A1$, OPA836, Texas Instrument) for a better signal-to-noise ratio and impedance matching in the signal transmission line.[5] On the input side, there is an additional resistor ($R2 = R9 = 10\Omega$) to stabilize the input. The value of the resistor on the output side ($R5 = R12 = 50\Omega$) matches the impedance with the cables used in this experiment. The voltage gain of the amplifier is equal to 1, determined by $R3 = R4 = R10 = R11 = 400\Omega$. This circuit part is assembled on a miniature circuit board (0.56 × 2.54 cm^2) and inserted into the probe shaft.

The part in red is for δn_e measurement. A relatively larger bias capacitor, $C1$ = 250 μF, is charged to the bias voltage of 30–35 V, prior to the plasma operation. A small capacitor, $C2$ = 1 μF, is connected in parallel to ensure that the bias voltage is maintained for high-frequency components. With these two capacitors, the V_- tip draws the ion saturation current during the MRX discharge that lasts about 1 ms. The voltage signal across a shunt resistor $R6 = 10\Omega$ is filtered by a high-pass filter, denoted by a green rectangle. The high-pass filter is designed to be electrically symmetric ($C3 = C4$ = 50 nF, $C5 = C6$ = 200 nF, $R7 = 100\Omega$) on both sides to minimize the common mode pickup. The value of the shunt resistor is optimized to have a good signal-to-noise ratio with a negligible voltage drop across it ($\lesssim$ 1 V). The filtered signal is connected to the same transformer for electrical isolation. The rest part of the circuit

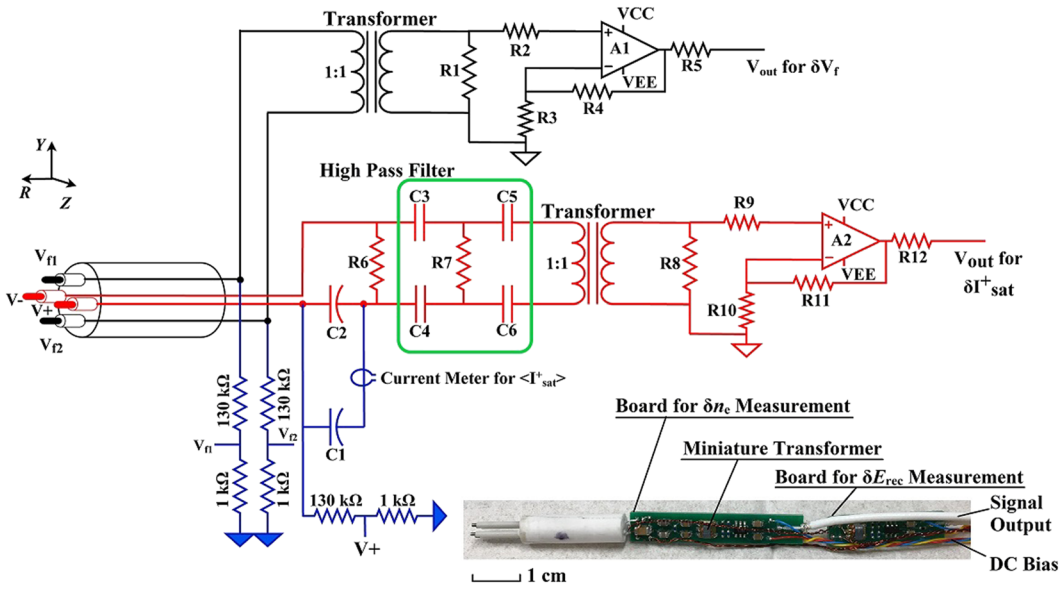

FIG. 1. Diagram for the probe tip configuration and measurement circuit. The part in black is for δE_{rec} measurement, while the part in red is for δn_e measurement. Two floating tips (V_{f1} and V_{f2}) are connected directly to a miniature transformer for measurements of E_{rec}. Two tips in red (V_+ and V_-) are connected to a shunt resistor ($R6 = 10\Omega$) through a bias capacitor ($C2$) for measurements of the ion saturation current. Inside the green rectangle is a high-pass filter that allows only the high-frequency fluctuation signal to reach a miniature transformer. The part in blue provides low-frequency (time-averaged) measurements of the electron temperature and density. The two floating tips are aligned along the Y (azimuthal) direction in MRX to measure fluctuations in the reconnection electric field component.

for δn_e measurement is the same as the circuit for δE_{rec} measurement. The circuit is also assembled on a miniature circuit board (0.56×3.81 cm^2) and inserted into the probe shaft.

The part in blue is a diagram for an external circuit that measures the average electron density and temperature. The voltage of V_{f1}, V_{f2}, and V_+ tips is reduced by voltage dividers and recorded by digitizers (2.5 MSPS) through buffer amplifiers (OPA633, Texas Instrument). The resistance of the voltage dividers needs to be large enough so that the current going through them can be neglected, compared to the ion saturation current (~ 0.2 A). We use 130 kΩ resistors to keep the current going through the dividers less than 1 mA. If the resistance is too big (>1 MΩ), the stray capacitance in the circuit impacts on measurements. The high-frequency signals are recorded by a high-bandwidth (300 MHz) oscilloscope. The average saturation current is measured by a current monitor (Model No. 2877, Pearson Electronics).

C. Probe applicability analysis and construction

High-frequency measurements in plasma require a careful design of the circuit and the probe. The temporal resolution of a Langmuir probe, for example, is limited by various transient effects in the sheath since the theory of Langmuir probes is based on a stationary sheath.[18] It is important to verify that the target frequency (10 MHz) of measurements is lower than the frequency limits from the transient effects. Without a voltage sweeping, there are four relevant frequencies—$f_{\text{sheath transit}}$, $f_{\text{sheath formation}}$, $f_{\text{sheath cap}}$, and $f_{\text{stray cap}}$. The sheath transit frequency, $f_{\text{sheath transit}}$, is related to the time required for a particle to traverse the entire sheath. The sheath formation frequency, $f_{\text{sheath formation}}$, is related to the time for a steady sheath to form around the probe. Both $f_{\text{sheath cap}}$ and $f_{\text{stray cap}}$ are related to capacitive effects associated with the sheath capacitance and stray capacitance, which causes leakage for high frequency signals. The bound frequencies for these effects are estimated by[18]

$$f_{\text{sheath transit}} \approx 2 f_{\text{pi}}, \tag{5}$$

$$f_{\text{sheath formation}} \approx \pi \left(3 + \frac{r_p}{\lambda_D}\right)^{-1} M_\infty f_{\text{pi}}, \tag{6}$$

$$f_{\text{sheath cap}} = 4\pi \exp\left(-\frac{1}{2}\right)\left(\frac{T_e}{\Delta V_B}\right) f_{\text{pi}}, \tag{7}$$

$$f_{\text{stray cap}} = 2\pi \exp\left(-\frac{1}{2}\right)\left(\frac{A\epsilon_0}{C_{\text{stray}}\lambda_D}\right)\left(\frac{T_e}{\Delta V_B}\right) f_{\text{pi}}, \tag{8}$$

where f_{pi} is the ion plasma frequency, r_p is the radius of each probe tip, λ_D is the Debye length, M_∞ is the Mach number (set $M_\infty = 1$ as ensured by the presheath), ΔV_B is the bias voltage of the probe, ϵ_0 is the vacuum permittivity, and C_{stray} is the stray capacitance of all the coaxial cables.

Two of the bound frequencies are related to the dimension of the probe tip; the size of the probe tip should be large enough to make both $f_{\text{sheath formation}}$ and $f_{\text{stray cap}}$ larger than 10 MHz. The dimension of the cylindrical tip is $r_p = 0.38$ mm and $h = 1.0$ mm (h is the height of the cylinder). With these dimensions and the parameters in Table I, the range of four bound frequencies is obtained. As summarized in Table II, all values are larger than the target frequency of 10 MHz.

TABLE II. Bound frequencies from transient effects of a Langmuir probe.

Parameters	Values
$f_{\text{sheath transit}}$ (MHz)	660–2100
$f_{\text{sheath formation}}$ (MHz)	41–63
$f_{\text{sheath cap}}$ (MHz)	360–3400
$f_{\text{stray cap}}$ (MHz)	200–3700

Potential issues regarding the miniature transformer have also been examined. First, in our previous work, it has been confirmed that the local perturbations caused by the core fall off sharply with an increase in distance and should not adversely effect fluctuation measurements.[5] Second, the functionality of the transformer up to 500 G has been tested by applying a 10 MHz signal to the transformer under a DC magnetic field (> 500 G) from two permanent magnets. We confirm that the transformer is not saturated and the deformation of the waveform is negligible. We have also confirmed that the possible pickup of magnetic field fluctuations by the transformer is negligible.

The probe may pick up a large (~ 100 V/m) common mode signal. To reduce the common mode signal as much as possible, we use twisted pairs or coaxial cables for all the connections, place two circuit boards close to the probe tip for reducing the length of wires from tips, employ a symmetric high-pass filter, choose small passive and active components on the boards, and insert the circuit boards inside a stainless steel probe shaft for shielding.

After this extensive design, the probe has been constructed. As shown in the photograph in Fig. 1, four tungsten probe tips are inserted into four alumina tubes fixed in an alumina base and connected to two miniature printed circuit boards via coated wires. The board in the middle of the photo is for the δn_e measurement, while that on the right is for the δE_{rec} measurement. The whole probe, including the probe shaft and the circuit boards, is inserted into the plasma along the R-axis. The probe tips are perpendicular to the Y–Z plane, while the two tips V_{f1} and V_{f2} are placed along the Y-axis to measure δE_{rec} (E_{rec} is along the Y-axis) and the other two tips V_+ and V_- are placed along the Z-axis to measure δn_e. The orientation of the four probe tips is centrosymmetric in the Y–Z plane so that this probe can be regarded as measuring δE_{rec} and δn_e at the same position. The tip separation (~ 2 mm) is about twice the tip size (diameter 0.76 mm) to minimize possible shadow effects. It should be noted that the probe design is based on the assumption that the wavelength of modes causing fluctuations is larger than the separation of tips; if the wavelength becomes comparable to the tip separation along either the Y or Z direction, the probe will not have good measurements of the corresponding fluctuating quantity. The output signals are connected with two white coaxial cables with an impedance of 50 Ω. The DC bias voltages for the amplifiers are provided by three twisted wires (+2.5, −2.5 V, and ground). All the wires, cables, alumina base, and circuit boards are inserted into a stainless steel shaft and sealed with a vacuum-compatible epoxy resin.

D. LT-Spice modeling and calibration

Figure 2 shows the circuit diagram of the LT-Spice modeling for δn_e measurements, which is the unique part of this probe. The design for the electric field fluctuations is very similar to that in Ref. 5. A sinusoidal current source ($I1$) is inserted to model the ion saturation current; it should be noted that if $I1$ is replaced by a sinusoidal voltage source, the output voltage is negligible. This confirms that this circuit is designed to detect fluctuations in the ion saturation current rather than fluctuations in the plasma potential. The left part of I1 represents circuit components in the external circuit (blue part in Fig. 1). Here, R_C is the measured resistance of all cables and connections and $L1$ and R_0 are the equivalent inductance and resistance associated with the current measurement by the Pearson monitor.

An actual circuit board measurement is also needed to make sure this design meets our requirements. After the probe was constructed, the test is taken by applying a test sinusoidal signal to the probe tips and then measuring the output signal of the whole probe. Through changing the frequency of the test signal, we can obtain the amplitude and phase response in the frequency range from 10 kHz to 10 MHz. For the δE_{rec} measurement, the probe is trying to pick up a voltage signal from the plasma potential, so the test signal is a sinusoidal voltage signal from a digital signal generator. For the δn_e measurement, the probe is trying to collect the ion saturation current. Hence, the test signal should come from a sinusoidal current source. We use a Pearson current monitor to measure the current going through the probe tips so that we can make the amplitude of the test signal stay the same each time we adjust the frequency. For both measurements, the output signal is detected by a digital oscilloscope. The amplitudes of the test signal and the output signal, as well as the phase shift between the output and the test signal, are recorded to obtain the amplitude response and phase response.

The results from the Spice modeling are compared with actual measurements, as shown in Fig. 3. Here, V_{in} is the voltage drop across the shunt resistor. As shown in Fig. 3(a), signals under 10 kHz are significantly reduced due to the high-pass filter, while amplitudes of signals over 0.1 MHz are maintained. There is a

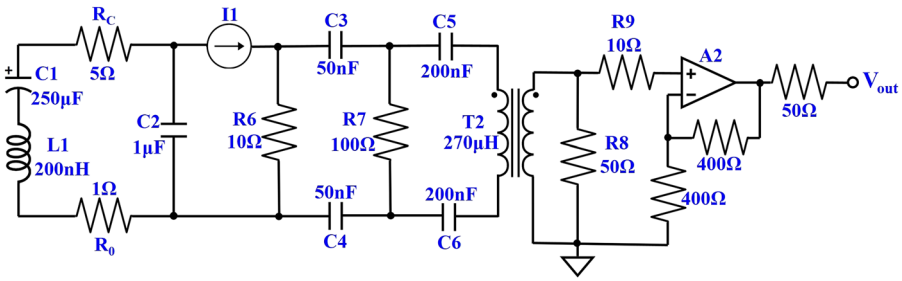

FIG. 2. LT-Spice modeling for δn_e measurement. $I1$ is a current source being used to simulate the plasma. R_C is the resistance of all the cables. $L1$ and R_0 are the equivalent inductance and resistance caused by the current meter for $\langle I_{sat}^{+} \rangle$.

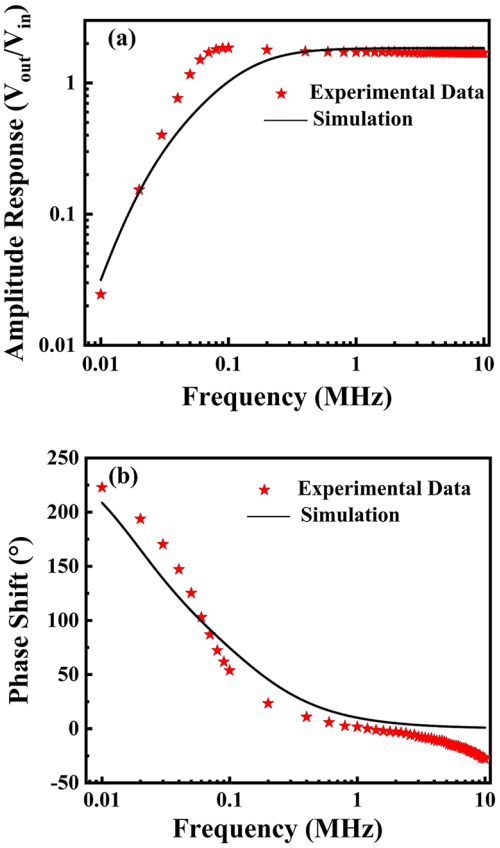

FIG. 3. Comparison of amplitude response and phase response between simulation and the real board test of the circuit for δn_e measurement. (a) The amplitude response and (b) the phase response. The black solid lines represent the simulation results, and the red stars represent the test results. The measurement error is small so that the error bars are not shown in the results. Here, V_{in} is the voltage on the shunt resistor, which can be obtained by $V_{in} = I_{in} \times R6$. I_{in} is the current passing through the probe tips measured by a Pearson current meter.

noticeable discrepancy between expected and measured values around 0.1 MHz; the actual circuit performance exceeds expectation since the slope of the response curve is sharper with a similar cut-off frequency. The cause of this discrepancy is not fully understood, but it is probably related to an internal resonance associated with the transformer.

Figure 3(b) shows the phase shift between the input and output signals. The circuit shows a negligible phase shift for signals with a frequency of 0.1–4 MHz. At higher frequencies, the phase shift becomes unexpectedly larger, which is caused by parasitic inductance and capacitance existing in the circuit board. If necessary, the signal obtained in the experiment can be processed via the Fourier transform to compensate the phase shift by the circuit.

The performance of the circuit for δE_{rec} measurements has been also verified. As shown in Fig. 4, the circuit performs as a voltage follower; the amplitude of the output signal is almost consistent with the input signal, only slightly amplified when the frequency is higher than 8 MHz. The phase response is linear, which means that the time delay for all frequencies is a constant (13 ns). It is

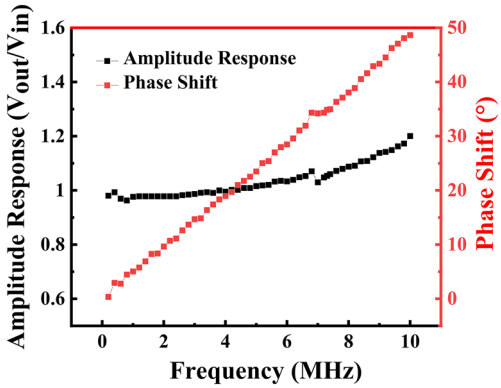

FIG. 4. Test results for δE_{rec} measurement. The black dotted line represents the amplitude response, and the red dotted line represents the phase response. The V_{out}/V_{in} value is approximately equal to 1, only a slight increase when the frequency is higher than 8 MHz, which means the signals can pass through the circuit without any obstructions. The phase response is almost linear, which means the delay time of the output signal is a constant for all frequencies.

worth noting that there is a drip around 7 MHz in both amplitude and phase responses. We suspect that these disturbances are caused by resonances in the circuit from parasitic inductance and capacitance. However, the overall circuit performance satisfies the requirements of the experiments—the capability to measure high-frequency fluctuations up to 10 MHz without significant phase delays.

III. EXAMPLE DATA IN MRX

The constructed probe (Fig. 1) has been used to obtain data during reconnection experiments in MRX. Figure 5(a) shows the reconnection geometry in MRX at $t = 326\,\mu$s. The color contours show the 2D profile of the out-of-plane current density, while the black lines are contours of the poloidal flux, representing the magnetic field.[10] At this time, the current sheet is located around $(R, Z) = (38, 0)$ cm. The red asterisk indicates the location of the probe $[(R, Z) = (37.5, 0)\,\text{cm}]$. Due to the radially inward motion of the current sheet, the relative distance between the current sheet and the probe changes over time.[19] As a result, the local lower hybrid frequency (f_{LH}) changes over time, as shown in Fig. 5(e). The sharp decrease in f_{LH} after $t = 330\,\mu$s is caused by the approach of the X-point to the probe.

In this plasma, there is a strong density asymmetry across the current sheet, and the density is about five times larger on the upper side ($R \sim 45$ cm), compared to the inboard side ($R \sim 30$ cm). Figure 5(b) shows the 2D profile of the out-of-plane magnetic field component. Due to the density asymmetry, the profile is almost bipolar.[14] Under this density asymmetry, the quasi-electrostatic LHDW is unstable near the low-density side separatrix.[5,14,20–24] Near the X-point, on the other hand, the LHDW becomes stable due to the stabilization by high β.[5,25] Because the probe has only one measurement point, the probe cannot be used to identify the wave mode; we have chosen the experimental condition well-known for generating the quasi-electrostatic lower hybrid drift waves to test the performance of the probe.

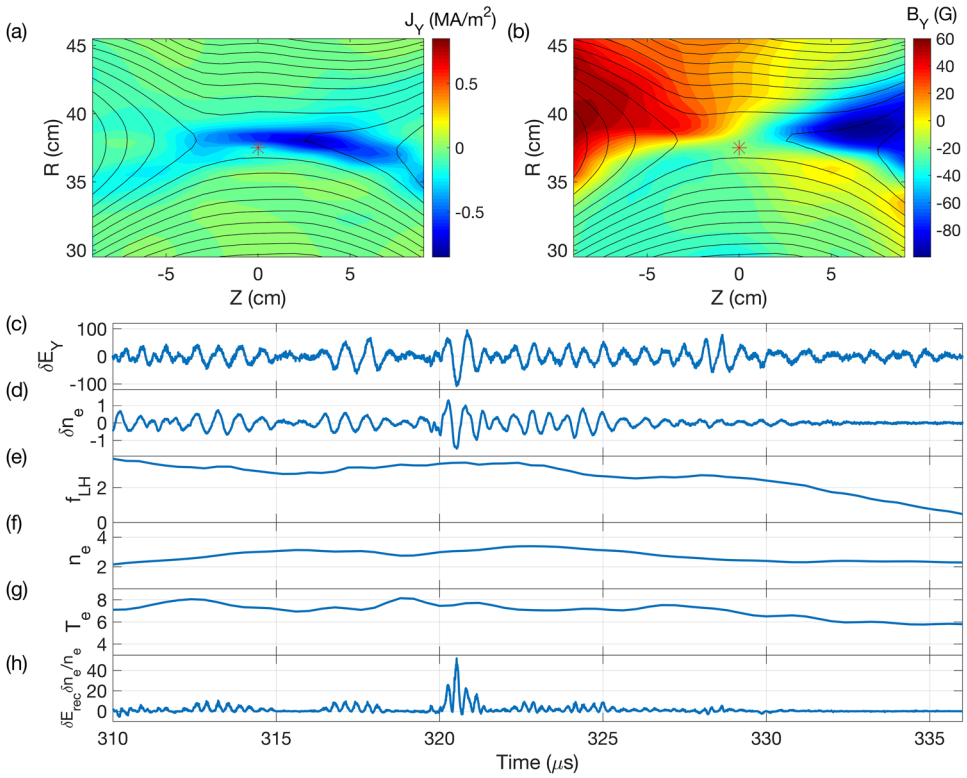

FIG. 5. Data from the constructed electrostatic probe during reconnection experiments in MRX. (a) 2D profiles of the out-of-plane current (color contours) with the poloidal flux contours (black lines) representing the magnetic field lines at 326 μs. The red asterisk indicates the location of the probe. (b) 2D profile of the out-of-plane magnetic field at 326 μs. The upper side ($R > 37.5$ cm) has a higher density. (c) Time series of δE_{rec} in V/m. Wave activity near the lower hybrid frequency (~ 2 MHz) is detected, while the probe stays near the reconnection site. The amplitude of the fluctuation is comparable to the mean reconnection electric field ($\langle E_{rec} \rangle \sim 100$ V/m). (d) Time series of δn_e in 10^{13} cm^{-3} during the quasi-steady reconnection period. Significant density fluctuations correlated with the electric field fluctuations are observed. (e) Time series of the lower hybrid frequency f_{LH}. A sharp decrease in f_{LH} is observed as the approach of the X-point to the probe. (f) Profile of the average density ($\langle n_e \rangle$) in 10^{13} cm^{-3}. (g) Profile of the electron temperature (T_e) in eV. (h) Profile of $\delta E_{rec} \delta n_e / \langle n_e \rangle$. Due to the positive correlation between δE_{rec} and δn_e, this term is mostly positive, indicating that the wave is capable of generating anomalous resistivity.

Figures 5(c) and 5(d) show data of δE_{rec} and n_e from the same MRX discharge. The probe detects high-frequency (~ 2 MHz) fluctuations of both δE_{rec} and n_e. This frequency is slightly below the local lower hybrid frequency. Moreover, these fluctuations mostly disappear when the X-point approaches the probe and the local plasma β becomes high. These features are consistent with quasi-electrostatic lower hybrid drift waves that have been extensively studied under the same condition in MRX[5,14] and in space.[24] To demonstrate the probe's functionality, data of both electron density and temperature from the probe are also presented in Figs. 5(f) and 5(g), respectively. We have also verified the noise from capacitor bank operations is negligible during the time of measurements by looking at signals from vacuum operation.

From these measurements, the wave-associated anomalous drag can be directly estimated, as shown in Fig. 5(h). Due to the positive correlation between δE_{rec} and δn_e, $\delta E_{rec} \delta n_e / \langle n_e \rangle$ is mostly positive throughout the measurement time, indicating the presence of anomalous drag there. These positive anomalous drag is consistent with recent space observations.[24] Strictly speaking, the anomalous drag, D, in Eq. (1) requires spatial averaging of $\delta E_{rec} \delta n_e$,[8] which is not possible due to the limited number of measurements. However, the probe can provide the time series of $\delta E_{rec} \delta n_e / \langle n_e \rangle$. With a proper temporal averaging and spatial scan of the probe, the profile of D near the reconnection region can be obtained.

IV. SUMMARY AND CONCLUSION

We have developed a special four-tip electrostatic probe, which can simultaneously measure high-frequency fluctuations in the electric field and electron density. The probe also provides data on the (average) electron density and temperature. The target frequency range is 0.1–10 MHz, and we have designed probe tips to ensure that all bound frequencies of transient effects of a Langmuir probe are above the target frequency. The circuits for high-frequency measurements are also designed to meet the frequency requirement. To minimize the noise pickup through the transmission line, the circuits are assembled on miniature circuit boards and located near the probe tips.

We have verified the functionality of the high-frequency circuits with sinusoidal signals. Over the range of 0.1–10 MHz, the

amplitude response is close to unity and the phase shift is less than 30°. With precise calibrations of the phase shift and amplitude response, this probe can measure fluctuations up to 200 MHz, which is limited by the analog bandwidth of the amplifier (205 MHz). The transformer has a 3 dB bandwidth of 0.05–450 MHz. Finally, we demonstrate the probe's capability of measuring δE_{rec} and δn_{e} in MRX discharges. The probe successfully detects high-frequency (~2 MHz) fluctuations associated with the quasi-electrostatic lower hybrid drift wave. With simultaneous measurements of δE_{rec}, δn_{e}, T_{e}, and n_{e}, it is possible to estimate the anomalous drag and the classical resistivity at the probe location, which will be useful to understand impacts from various waves and wave-associated electron heating.

ACKNOWLEDGMENTS

This work was supported by the DOE (Contract No. DE-AC0209CH11466), the National Natural Science Foundation of China (NNSFC) (Contract No. 11975163), the Priority Academic Program Development of Jiangsu Higher Education Institutions (PAPD), and the Program for Graduates Research and Innovation in University of Jiangsu Province (Contract No. KYCX17-2025).

DATA AVAILABILITY

The data that support the findings of this study are openly available in the DataSpace of Princeton University at http://arks.princeton.edu/ark:/88435/dsp01x920g025r.

REFERENCES

[1]H. Ji, H. Toyama, K. Yamagishi, S. Shinohara, A. Fujisawa, and K. Miyamoto, "Probe measurements in the REPUTE-1 reversed field pinch," Rev. Sci. Instrum. **62**, 2326–2337 (1991).
[2]S.-L. Chen and T. Sekiguchi, "Instantaneous direct-display system of plasma parameters by means of triple probe," J. Appl. Phys. **36**, 2363–2375 (1965).
[3]S. Majeski, J. Yoo, S. Zweben, and M. Yamada, "Detection of an electron beam in a high density plasma via an electrostatic probe," Plasma Phys. Controlled Fusion **60**, 075001 (2018).
[4]J. Yoo, M. Yamada, H. Ji, J. Jara-Almonte, and C. E. Myers, "Bulk ion acceleration and particle heating during magnetic reconnection in a laboratory plasma," Phys. Plasmas **21**, 055706 (2014).
[5]T. A. Carter, H. Ji, F. Trintchouk, M. Yamada, and R. M. Kulsrud, "Measurement of lower-hybrid drift turbulence in a reconnecting current sheet," Phys. Rev. Lett. **88**, 015001 (2001).
[6]H. Ji, S. Terry, M. Yamada, R. Kulsrud, A. Kuritsyn, and Y. Ren, "Electromagnetic fluctuations during fast reconnection in a laboratory plasma," Phys. Rev. Lett. **92**, 115001 (2004).
[7]F. S. Mozer, M. Wilber, and J. F. Drake, "Wave associated anomalous drag during magnetic field reconnection," Phys. Plasmas **18**, 102902 (2011).
[8]H. Che, "How anomalous resistivity accelerates magnetic reconnection," Phys. Plasmas **24**, 082115 (2017).
[9]N. Benjamin, "High-impedance capacitive divider probe for potential measurements in plasmas," Rev. Sci. Instrum. **53**, 1541–1543 (1982).
[10]M. Yamada, H. Ji, S. Hsu, T. Carter, R. Kulsrud, N. Bretz, F. Jobes, Y. Ono, and F. Perkins, "Study of driven magnetic reconnection in a laboratory plasma," Phys. Plasmas **4**, 1936–1944 (1997).
[11]H. Ji, M. Yamada, S. Hsu, and R. Kulsrud, "Experimental test of the Sweet-Parker model of magnetic reconnection," Phys. Rev. Lett. **80**, 3256 (1998).
[12]T. D. Tharp, M. Yamada, H. Ji, E. Lawrence, S. Dorfman, C. E. Myers, and J. Yoo, "Quantitative study of guide-field effects on Hall reconnection in a laboratory plasma," Phys. Rev. Lett. **109**, 165002 (2012).
[13]J. Jara-Almonte, H. Ji, M. Yamada, J. Yoo, and W. Fox, "Laboratory observation of resistive electron tearing in a two-fluid reconnecting current sheet," Phys. Rev. Lett. **117**, 095001 (2016).
[14]J. Yoo, M. Yamada, H. Ji, J. Jara-Almonte, C. E. Myers, and L.-J. Chen, "Laboratory study of magnetic reconnection with a density asymmetry across the current sheet," Phys. Rev. Lett. **113**, 095002 (2014).
[15]J. P. Sheehan and N. Hershkowitz, "Emissive probes," Plasma Sources Sci. Technol. **20**, 063001 (2011).
[16]I. H. Hutchinson, *Principles of Plasma Diagnostics*, 2nd ed. (Cambridge University Press, Cambridge, UK, 2005).
[17]I. H. Hutchinson, "Ion collection by a sphere in a flowing plasma: I. Quasineutral," Plasma Phys. Controlled Fusion **44**, 1953 (2002).
[18]R. B. Lobbia and A. D. Gallimore, "Temporal limits of a rapidly swept Langmuir probe," Phys. Plasmas **17**, 073502 (2010).
[19]J. Yoo and M. Yamada, "Experimental evaluation of common spacecraft data analysis techniques for reconnection region analysis in a laboratory plasma," J. Geophys. Res. **117**, A12202, https://doi.org/10.1029/2012ja017742 (2012).
[20]V. Roytershteyn, W. Daughton, H. Karimabadi, and F. S. Mozer, "Influence of the lower-hybrid drift instability on magnetic reconnection in asymmetric configurations," Phys. Rev. Lett. **108**, 185001 (2012).
[21]C. Norgren, A. Vaivads, Y. V. Khotyaintsev, and M. André, "Lower hybrid drift waves: Space observations," Phys. Rev. Lett. **109**, 055001 (2012).
[22]J. Yoo, J. Jara-Almonte, E. Yerger, S. Wang, T. Qian, A. Le, H. Ji, M. Yamada, W. Fox, E.-H. Kim, L.-J. Chen, and D. J. Gershman, "Whistler wave generation by anisotropic tail electrons during asymmetric magnetic reconnection in space and laboratory," Geophys. Res. Lett. **45**, 8054–8061, https://doi.org/10.1029/2018gl079278 (2018).
[23]J. Yoo, S. Wang, E. Yerger, J. Jara-Almonte, H. Ji, M. Yamada, L.-J. Chen, W. Fox, A. Goodman, and A. Alt, "Whistler wave generation by electron temperature anisotropy during magnetic reconnection at the magnetopause," Phys. Plasmas **26**, 052902 (2019).
[24]J. Yoo, J.-Y. Ji, M. V. Ambat, S. Wang, H. Ji, J. Lo, B. Li, Y. Ren, J. Jara-Almonte, L.-J. Chen, W. Fox, M. Yamada, A. Alt, and A. Goodman, "Lower hybrid drift waves during guide field reconnection," Geophys. Res. Lett. **47**, e2020GL087192, https://doi.org/10.1029/2020gl087192 (2020).
[25]R. Davidson, N. Gladd, C. Wu, and J. Huba, "Effects of finite plasma beta on the lower-hybriddrift instability," Phys. Fluids **20**, 301 (1977).